JACS
JOURNAL OF THE AMERICAN CHEMICAL SOCIETY

Communication

pubs.acs.org/JACS

Highly Efficient Red-Light Emission in An Organic–Inorganic Hybrid Ferroelectric: (Pyrrolidinium)$MnCl_3$

Yi Zhang,[†] Wei-Qiang Liao,[†] Da-Wei Fu,[†] Heng-Yun Ye,[†] Zhong-Ning Chen,[‡] and Ren-Gen Xiong*[,†]

[†]Ordered Matter Science Research Center, Southeast University, Nanjing 211189, P. R. China

[‡]Fujian Institute of Research on the Structure of Matter, The Chinese Academy of Sciences, Fuzhou, Fujian 350002, China

Supporting Information

ABSTRACT: Luminescence of ferroelectric materials is one important property for technological applications, such as low-energy electron excitation. However, the vast majority of doped inorganic ferroelectric materials have low luminescent efficiency. The past decade has envisaged much progress in the design of both ferroelectric and luminescent organic–inorganic hybrid complexes for optoelectronic applications. The combination of ferroelectricity and luminescence within organic–inorganic hybrids would lead to a new type of luminescent ferroelectric multifunctional materials. We herein report a hybrid molecular ferroelectric, (pyrrolidinium)$MnCl_3$, which exhibits excellent ferroelectricity with a saturation polarization of 5.5 $\mu C/cm^2$ as well as intense red luminescence with high quantum yield of 56% under a UV excitation. This finding may extend the application of organic–inorganic hybrid compounds to the field of ferroelectric luminescence and/or multifunctional devices.

The research and applications of luminescent materials have been changing our lives importantly. Among these promising materials, luminescent ferroelectrics are unique, e.g., for application in low-energy electron excitation. For example, the Al^{3+}-added $SrTiO_3$:Pr^{3+} with a perovskite structure shows red cathodoluminescence, which can be excited at a low anode voltage; even below 10 V.[1] The cathodoluminescence at such a low accelerating anode voltage makes this material attractive for potential applications in flat-panel display, field emission display (FED) and vacuum fluorescent displays.[1,2] However, the vast majority of these materials have low luminescent efficiency.

Along with the development and applications of organic–inorganic hybrid compounds in various fields in the past decade, a large number of luminescent materials based on hybrid organic–inorganic hybrid compounds have been developed because they combine facile synthesis with intriguing and tunable optical properties.[3] These advantages make them suitable for a variety of low-cost optoelectronic devices, such as light emitting diodes[4] and solar cells.[5] Meanwhile, much progress has been achieved in ferroelectricity in organic–inorganic hybrid compounds.[6] In this context, it is worthy to combine ferroelectricity and luminescence within organic–inorganic hybrids. This can not only realize tunable luminescence properties but also may lead to potential multifunctional optoelectronic device applications such as integrated optical sensors.

In the course of our systematic search for new molecule-based ferroelectrics, such as high-temperature molecular ferroelectrics,[7] molecular ferroelectric thin film,[8] and anomalous photovoltaic effect,[9] we have found that hybrid metal halide perovskite-type compounds with general formula of AMX_3 (A = organic ammonium cation, M = divalent metal, X = halogen) exhibit excellent ferroelectricity.[9,10] Such hexagonal stacking perovskites involve a large class of compounds (M = Mn, Fe, Co, Ni, Cu, Cr, or V; X = Cl or Br).[11] Among them, the Mn-compounds have been discovered to fluoresce brightly due to the existence of the luminous activator Mn^{2+} ion.[12] By deliberate selection of organic cations, we have designed a new 2-H hexagonal stacking perovskite-type ferroelectric, (pyrrolidinium)$MnCl_3$ (**1**) (Figure S1), which exhibits intense red luminescence under a UV excitation. Here, we describe its preparation, structural phase transition, and ferroelectric and photoluminescence properties.

Compound **1** was prepared as pink rod single crystals up to 3 × 3 × 15 mm^3 in size by slow evaporation of stoichiometric amounts of $MnCl_2$ and pyrrolidinium chloride in a concentrated HCl solution. Compound **1** was found to undergo a structural phase transition by differential scanning calorimetry (DSC) measurements. As shown in Figure 1a, the DSC curve shows two peaks at 291 and 295 K in the cooling and heating runs, respectively, indicating a reversible structural phase transition. For convenience, we label the phase above 295 K as the high-temperature phase (HTP) and the phase below 291

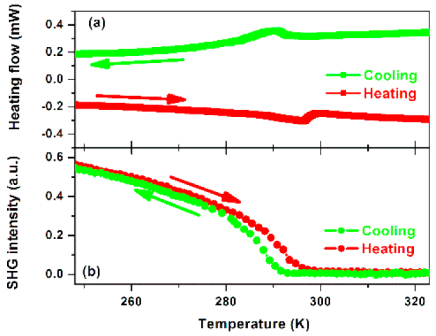

Figure 1. Thermal analysis (a) and SHG characterization (b) for the structural phase transition in **1**.

Received: February 13, 2015
Published: March 25, 2015

DOI: 10.1021/jacs.5b01680
J. Am. Chem. Soc. 2015, 137, 4928–4931

K as the low-temperature phase (LTP). Both phases are orthorhombic with similar cell constants.[13] Systematic absences for both the phases point to two most possible space groups: $Cmc2_1$ and $Cmcm$. The refinements for each phase with the two space groups respectively converge very well. At this stage, we measured the response of second harmonic generation (SHG) signal of **1** as a function of temperature. As shown in Figure 1b, the SHG activity changes at around 293 K. Above 293 K, the SHG shows zero intensity of the signal. As temperature further decreases from 293 K, the signal intensity increases gradually. The continuous increase reveals the continuous characteristic for a second-order transition. The significant change in SHG activity indicates that the HTP is centrosymmetric, while the LTP is non-centrosymmetric because only solids with non-centrosymmetric space groups are SHG active.[14] We finally refined the structure of the LTP at 273 K in the polar space group $Cmc2_1$ and the structure of the HTP at 313 K in the centrosymmetric $Cmcm$. This also accords with the requirement of the Aizu rule[15] for a $mmmFmm2$ ferroelectric transition.

The crystal structures of the two phases are similar except the orientation of the organic pyrrolidinium cation (Figure 2). The

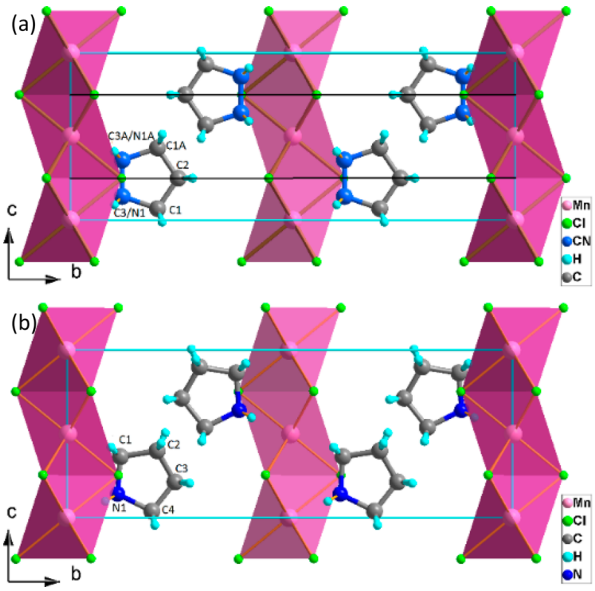

Figure 2. Projects of the HTP (a) and LTP (b) of **1** along the common *a*-axis, showing the similarities of the crystal structures and the differences of orientation states of the organic pyrrolidinium cations. The dark lines in (a) indicate the crystallographic mirror planes.

crystal structures consist of linear chains of face-sharing $MnCl_6$ octahedra separated by pyrrolidinium cations. The Mn−Cl bond distances (2.525(3)−2.595(4) Å) and Cl−Mn−Cl bond angle (2.595(4)−97.94(8)°) are comparable to those in other analogues, such as $(CH_3)_2NH_2MnCl_3$,[16] $[Me_3NH][MnCl_3]$,[17] and $(CH_3)_4NMnCl_3$.[12] In the HTP, the pyrrolidinium cation is located on a special position with $mm2$ symmetry. The five-membered ring was modeled as planar, and the ring plane is superimposed on one of the two crystallographic mirror planes. The symmetry required by the other mirror plane perpendicular to the ring plane is satisfied by the 2-fold orientational disorder with the N atom and a C atom distributing over the mirror plane. In the LTP, the requirement of this mirror symmetry is lost, and thus, the atoms at the positions of C1 and N1 (Figure 2b) were assigned to a C and N atom, respectively. This model indicates that the LTP is formed by reorientation of the organic cations, and the transition is of the order−disorder type. In the DSC measurements, the transition enthalpy was estimated to be 26.37 J/mol. This corresponds to an entropy gain ΔS = 0.0089 J mol^{-1} K^{-1}, close to R ln 1.01 (R is the gas constant), completely deviating from the model of order−disorder transition in the structural determination. This means that the ordering of the organic cations is completed in a wide temperature range. For each cation, the ordering gives rise to a displacement of 0.7238 Å of the center of the positive charge (Figure 2). This contributes a polarization of 5.4 μC/cm^2 to the spontaneous polarization calculated from a point charge model (Supporting Information), which is close to the experimental value (5.5 μC/cm^2) of the saturation polarization at 253 K and 50 Hz (Figure 3c). For more structural information, see Figure S4 in the Supporting Information.

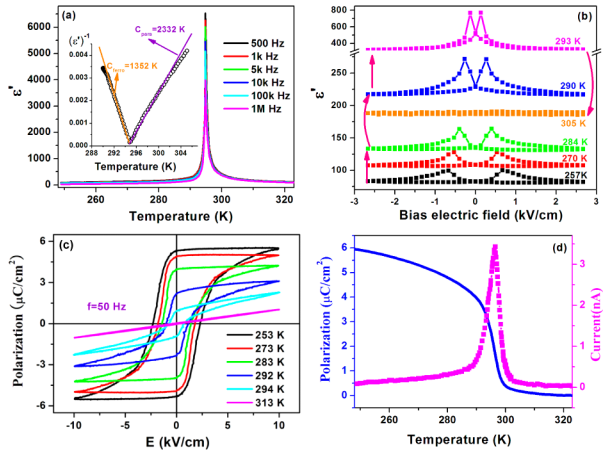

Figure 3. Ferroelectric properties in **1**. (a) Dielectric responses at various frequencies with variation of the temperature. Inset: the reciprocal dielectric constant $1/\varepsilon'$ at 500 Hz as a function of temperature. (b) Field dependence of the dielectric constant in both the paraelectric phase and the ferroelectric phase. (c) Polarization−electric field (P−E) hysteresis loops in the vicinity of T_c, measured by a Sawyer−Tower circuit. (d) Polarization determined by integration of the pyroelectric current.

The structural analysis on the transition from a centrosymmetric phase to a polar phase suggests a paraelectric-to-ferroelectric transition.[18] This is evident by the giant dielectric anomalies. As shown in Figure 3a, the giant λ-shape dielectric responses at T_c = 295 K with the peak values 4800−6500 of the real part ε' of the complex constant ($\varepsilon = \varepsilon' - i\varepsilon''$, ε'' is the imaginary part) in the low frequency range are characteristic of a ferroelectric transition.[18] Another character of the dielectric response for a ferroelectric material is that in the vicinity of paraelectric−ferroelectric transition temperature T_c, ε' shows Curie−Weiss behavior, that is, $\varepsilon' = C_{para}/(T - T_0)(T > T_c)$ or $C_{ferro}/(T_0' - T)(T < T_c)$. As shown in the inset of Figure 3a, the dielectric response at 500 Hz follows Curie−Weiss law very well. The ratio of C_{para}/C_{ferro} (Supporting Information, Table S1) at different frequencies is close to the theoretical value (C_{para}/C_{ferro} = 2) expected for a second-order transition, consistent with the SHG measurements. Ferroelectric materials also distinguish themselves from ordinary dielectric materials in the dielectric nonlinearity under a strong field, that is, a strong bias field leads to subloops of nonlinear dielectric constant in ferroelectrics. In **1**, the field dependence of the dielectric

DOI: 10.1021/jacs.5b01680
J. Am. Chem. Soc. 2015, 137, 4928−4931

constant in the LTP shows a butterfly loop (Figure 3b), as observed in other ferroelectrics.

The ferroelectricity and appearance of electric polarization were further confirmed by the measurements of polarization−electric field (P−E) hysteresis loops and pyroelectric effect. Figure 3c shows the (P−E) hysteresis loops at various temperatures. At 313 K in the high-temperature paraelectric phase, the polarization response to the applied field is linear, as expected for ordinary dielectrics under a smaller field. Below T_c, nonzero remnant polarization (P_r) at zero field and hysteresis loops were observed. The saturation polarization (P_s) (obtained by extrapolation of the linear parts of the loops to zero field) and P_r increase as temperature decreases. At 253 K and 50 Hz, we obtained $P_s \approx P_r = 5.5\ \mu C/cm^2$ and coercive field (the intercept of the loop with the field axis) $E_c = 2.3$ kV/cm. P_s at 253 K is comparable to that for (3-pyrrolinium)$CdCl_3$[9] (5.1 $\mu C/cm^2$); greater than those for other analogues including $N(CH_3)_4CdBr_3$ (0.12 $\mu C/cm^2$),[19] $(C_5H_9NH_3)(CdCl_3)$ (1.7 $\mu C/cm^2$),[10] metal formates with general formula $[NH_4][M(HCOO)_3]$ (M = Zn, Mn, Co, Fe, Ni, Zn) (0.97−2.2 $\mu C/cm^2$),[6b,c] and some of recently developed small-molecule organic ferroelectrics[7a,20] (0.1−1.2 $\mu C/cm^2$);[20a−c] and smaller than those for several of the organic ferroelectrics (7−55 $\mu C/cm^2$).[7a,20d−f] Another feature of the ferroelectricity is the high-frequency polarization switching. As shown in Figure S5 (Supporting Information), the investigated shortest switching time is about 2×10^{-4} s, much shorter than those found in some pure organic ferroelectrics (about one second)[20e] and polymer materials (about 10^{-3} second).[21] The high performance of polarization switching was rarely observed in molecular ferroelectrics.

The appearance of spontaneous electric polarization will lead to detectable current when there is a circuit between the two polar surfaces of the crystal, which is called the pyroelectric effect. By integrating the pyroelectric current, we obtained the polarization as a function of temperature (Figure 3d). The increase of the polarization with temperature decreasing below T_c is continuous and follows the same path as that of the SHG signal (Figure 1b). The polarization values by integrating the pyroelectric current are consistent with those by the measurements of (P−E) hysteresis loops.

In addition to the ferroelectric properties, **1** shows intriguing luminescence properties. As shown in Figure 4a,c, the crystals of **1** is orange red and somewhat transparent under ambient light. When subjected to UV light, it shows intense red phosphorescence. The emission from such large single crystals indicates an origin from the bulk material. Practically, such emission from the bulk phase will not be affected by the size or the surface defect of the sample, unlike that of nanometer structures like quantum dots or wires. Figure 4e presents the absorption and emission spectra of **1**. In addition to absorption in the UV range, **1** shows strong absorption in the visible region centered at around 440 and 540 nm, respectively. The emission spectra were recorded with excitation wavelength of 540 nm. The red phosphorescence at about 640 nm is produced by octahedrally coordinated manganese, which is attributable to the $(t_{2g})^3(e_g)^2$−$(t_{2g})^4(e_g)^1$ electronic transition.[22] The emission wavelength is close to that of Pr^{3+}-doped $CaTiO_3$, while the full wave half-maximum (fwhm) is a bit larger. As expected, the fluorescence becomes brighter with decreasing temperature. The quantum yield at room temperature is 53.6% with the lifetime of 515 μs (Figures S6 and S7), which is high enough for applications in optoelectronic devices.

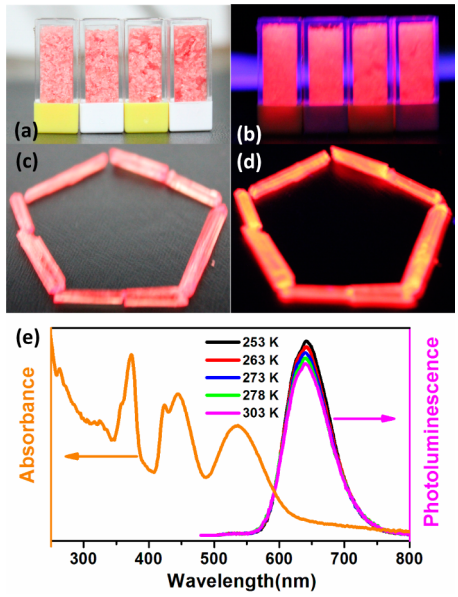

Figure 4. Photoluminescence properties of **1**. (,c) Crystals of **1** under ambient light. (b,d) Crystals of **1** under UV light. (e) Absorption and emission spectra of **1** at various temperatures.

In summary, we showed the highly efficient red emission in the hybrid 2-H hexagonal stacking perovskite-type ferroelectric: (pyrrolidinium)$MnCl_3$. This finding opens a new avenue for preparation of luminescent ferroelectric materials based on organic−inorganic hybrid compounds. As has been reported recently, such 2-H hexagonal stacking perovskite-type ferroelectrics are structurally tunable by modifying the template small-molecule organic ammonium cations and/or the bridging halogen atoms. Thus, it is possible to prepare high performance luminescent ferroelectric materials.

■ ASSOCIATED CONTENT

Supporting Information

Supplementary methods and Figures S1−S7. This material is available free of charge via the Internet at http://pubs.acs.org.

■ AUTHOR INFORMATION

Corresponding Author

*xiongrg@seu.edu.cn

Notes

The authors declare no competing financial interest.

■ ACKNOWLEDGMENTS

This work was supported by 973 project (2014CB932103), the National Natural Science Foundation of China (21290172, 91422301, and 21427801), and the Outstanding Young Teachers of Southeast University Research Fund.

■ REFERENCES

(1) Yamamoto, H.; Okamoto, S.; Kobayashi, H. *J. Lumin.* **2002**, *100*, 325.

(2) (a) Pizani, P. S.; Leite, E. R.; Pontes, F. M.; Paris, E. C.; Rangel, J. H.; Lee, E. J. H.; Longo, E.; Delega, P.; Varela, J. A. *Appl. Phys. Lett.* **2000**, *77*, 824. (b) Yamamoto, H.; Okamoto, S. *Displays* **2000**, *21*, 93.

(3) Xu, H.; Chen, R.; Sun, Q.; Lai, W.; Su, Q.; Huang, W.; Liu, X. *Chem. Soc. Rev.* **2014**, *43*, 3259.

(4) (a) Tan, Z. K.; Moghaddam, R. S.; Lai, M. L.; Docampo, P.; Higler, R.; Deschler, F.; Price, M.; Sadhanala, A.; Pazos, L. M.;

DOI: 10.1021/jacs.5b01680
J. Am. Chem. Soc. 2015, 137, 4928−4931

Credgington, D.; Hanusch, F.; Bein, T.; Snaith, H. J.; Friend, R. H. *Nat. Nanotechnol.* **2014**, *9*, 687. (b) Hang, X. C.; Fleetham, T.; Turner, E.; Brooks, J.; Li, J. *Angew. Chem., Int. Ed.* **2013**, *52*, 6753. (c) Dohner, E. R.; Jaffe, A.; Bradshaw, L. R.; Karunadasa, H. I. *J. Am. Chem. Soc.* **2014**, *136*, 13154. (d) Dohner, E. R.; Hoke, E. T.; Karunadasa, H. I. *J. Am. Chem. Soc.* **2014**, *136*, 1718.

(5) (a) Chen, C. Y.; Chen, J. G.; Wu, S.; Li, J. Y.; Wu, C. G.; Ho, K. C. *Angew. Chem., Int. Ed.* **2008**, *47*, 7342. (b) Pellet, N.; Gao, P.; Gregori, G.; Yang, T. Y.; Nazeeruddin, M. K.; Maier, J.; Gratzel, M. *Angew. Chem., Int. Ed.* **2014**, *53*, 3151. (c) Xing, G. C.; Mathews, N.; Sun, S. Y.; Lim, S. S.; Lam, Y. M.; Gratzel, M.; Mhaisalkar, S.; Sum, T. C. *Science* **2013**, *342*, 344.

(6) (a) Du, Z. Y.; Xu, T. T.; Huang, B.; Su, Y. J.; Xue, W.; He, C. T.; Zhang, W. X.; Chen, X. M. *Angew. Chem., Int. Ed.* **2015**, *54*, 914. (b) Xu, G. C.; Ma, X. M.; Zhang, L.; Wang, Z. M.; Gao, S. *J. Am. Chem. Soc.* **2010**, *132*, 9588. (c) Xu, G. C.; Zhang, W.; Ma, X. M.; Chen, Y. H.; Zhang, L.; Cai, H.-L.; Wang, Z. M.; Xiong, R.-G.; Gao, S. *J. Am. Chem. Soc.* **2011**, *133*, 14948. (d) Zhang, W.; Xiong, R.-G. *Chem. Rev.* **2012**, *112*, 1163. (e) Du, Z. Y.; Zhao, Y. P.; Zhang, W. X.; Zhou, H. L.; He, C. T.; Xue, W.; Wang, B. Y.; Chen, X. M. *Chem. Commun.* **2014**, *50*, 1989. (f) Samantaray, R.; Clark, R. J.; Choi, E. S.; Dalal, N. S. *J. Am. Chem. Soc.* **2012**, *134*, 15953. (g) Jain, P.; Ramachandran, V.; Clark, R. J.; Zhou, H. D.; Toby, B. H.; Dalal, N. S.; Kroto, H. W.; Cheetham, A. K. *J. Am. Chem. Soc.* **2009**, *131*, 13625. (h) Di Sante, D.; Stroppa, A.; Jain, P.; Picozzi, S. *J. Am. Chem. Soc.* **2013**, *135*, 18126. (i) Pan, L.; Liu, G.; Li, H.; Meng, S.; Han, L.; Shang, J.; Chen, B.; Platero-Prats, A. E.; Lu, W.; Zou, X. D.; Li, R. W. *J. Am. Chem. Soc.* **2014**, *136*, 17477. (j) Liu, C. M.; Xiong, R.-G.; Zhang, D. Q.; Zhu, D. B. *J. Am. Chem. Soc.* **2010**, *132*, 4044. (k) Stroppa, A.; Jain, P.; Barone, P.; Marsman, M.; Perez-Mato, J. M.; Cheetham, A. K.; Kroto, H. W.; Picozzi, S. *Angew. Chem., Int. Ed.* **2011**, *50*, 5847. (l) Stroppa, A.; Barone, P.; Jain, P.; Perez-Mato, J. M.; Picozzi, S. *Adv. Mater.* **2013**, *25*, 2284. (m) Tian, Y.; Stroppa, A.; Chai, Y. S.; Yan, L. Q.; Wang, S. G.; Barone, P.; Picozzi, S.; Sun, Y. *Sci. Rep.* **2014**, *4*, 6062. (n) Tian, Y.; Stroppa, A.; Chai, Y. S.; Barone, P.; Perez-Mato, M.; Picozzi, S.; Sun, Y. *Phys. Status Solidi R* **2015**, *9*, 62. (o) Draxl, C.; Nabok, D.; Hannewald, K. *Acc. Chem. Res.* **2014**, *47*, 3225.

(7) (a) Fu, D.-W.; Cai, H.-L.; Liu, Y. M.; Ye, Q.; Zhang, W.; Zhang, Y.; Chen, X. Y.; Giovannetti, G.; Capone, M.; Li, J. Y.; Xiong, R.-G. *Science* **2013**, *339*, 425. (b) Fu, D.-W.; Zhang, W.; Cai, H.-L.; Ge, J. Z.; Zhang, Y.; Xiong, R.-G. *Adv. Mater.* **2011**, *23*, 5658.

(8) Zhang, Y.; Liu, Y. M.; Ye, H.-Y.; Fu, D.-W.; Gao, W. X.; Ma, H.; Liu, Z. G.; Liu, Y. Y.; Zhang, W.; Li, J. Y.; Yuan, G. L.; Xiong, R.-G. *Angew. Chem., Int. Ed.* **2014**, *53*, 5064.

(9) Ye, H.-Y.; Zhang, Y.; Fu, D.-W.; Xiong, R.-G. *Angew. Chem., Int. Ed.* **2014**, *53*, 11242.

(10) Zhang, Y.; Ye, H.-Y.; Zhang, W.; Xiong, R.-G. *Inorg. Chem. Front.* **2014**, *1*, 118.

(11) Ackerman, J. F.; Cole, G. M.; Holt, S. L. *Inorg. Chim. Acta* **1974**, *8*, 323.

(12) Morosin, B.; Graeber, E. J. *Acta Crystallogr.* **1967**, *23*, 766.

(13) Crystal data for **1** at 313 K: $(C_4H_{10}N)(MnCl_3)$, M_r = 233.42, orthorhombic, *Cmcm*, a = 7.690(9), b = 17.32(2), c = 6.498(7) Å, V = 865.2(17) Å^3, Z = 4, D_c = 1.815 g cm^{-3}, R_1 ($I > 2\sigma(I)$) = 0.0429, wR_2 (all data) = 0.1261, μ = 2.37 mm^{-1}, S = 1.241. At 273 K: orthorhombic, $Cmc2_1$, a = 7.647(7), b = 17.249(15), c = 6.477(6) Å, V = 854.4(13) Å^3, Z = 4, D_c = 1.792 g cm^{-3}, R_1 ($I > 2\sigma(I)$) = 0.0339, wR_2 (all data) = 0.0872, μ = 2.4 mm^{-1}, S = 1.156.

(14) Zhao, S.; Gong, P.; Luo, S.; Bai, L.; Lin, Z.; Ji, C.; Chen, T.; Hong, M.; Luo, J. *J. Am. Chem. Soc.* **2014**, *136*, 8560.

(15) Aizu, K. *J. Phys. Soc. Jpn.* **1969**, *27*, 387.

(16) Caputo, R. E.; Willett, R. D. *Phys. Rev. B* **1976**, *13*, 3956.

(17) Ravindran, M.; Willey, G. R.; Drew, M. G. B. *Inorg. Chim. Acta* **1990**, *175*, 99.

(18) Lines, M. E.; Glass, A. M. *Principles and Applications of Ferroelectrics and Related Materials*; Oxford University Press: Oxford, U.K., 1977.

(19) Gesi, K. *J. Phys. Soc. Jpn.* **1990**, *59*, 432.

(20) (a) Horiuchi, S.; Kumai, R.; Tokunaga, Y.; Tokura, Y. *J. Am. Chem. Soc.* **2008**, *130*, 13382. (b) Horiuchi, S.; Kumai, R.; Tokura, Y. *Angew. Chem., Int. Ed.* **2007**, *46*, 3497. (c) Horiuchi, S.; Ishii, F.; Kumai, R.; Okimoto, Y.; Tachibana, H.; Nagaosa, N.; Tokura, Y. *Nat. Mater.* **2005**, *4*, 163. (d) Horiuchi, S.; Tokunaga, Y.; Giovannetti, G.; Picozzi, S.; Itoh, H.; Shimano, R.; Kumai, R.; Tokura, Y. *Nature* **2010**, *463*, 789. (e) Tayi, A. S.; Shveyd, A. K.; Sue, A. C. H.; Szarko, J. M.; Rolczynski, B. S.; Cao, D.; Kennedy, T. J.; Sarjeant, A. A.; Stern, C. L.; Paxton, W. F.; Wu, W.; Dey, S. K.; Fahrenbach, A. C.; Guest, J. R.; Mohseni, H.; Chen, L. X.; Wang, K. L.; Stoddart, J. F.; Stupp, S. I. *Nature* **2012**, *488*, 485. (f) Kagawa, F.; Horiuchi, S.; Minami, N.; Ishibashi, S.; Kobayashi, K.; Kumai, R.; Murakami, Y.; Tokura, Y. *Nano Lett.* **2014**, *14*, 239.

(21) Furukawa, T. *Phase Trans.* **1989**, *18*, 143.

(22) Orgel, L. E. *J. Chem. Phys.* **1955**, *23*, 1958.

DOI: 10.1021/jacs.5b01680
J. Am. Chem. Soc. 2015, 137, 4928−4931